Interfacially-adsorbed particles enhance the self-propulsion of oil droplets in aqueous surfactant

Journal:	*Soft Matter*
Manuscript ID	SM-ART-12-2020-002234.R3
Article Type:	Paper
Date Submitted by the Author:	22-Jun-2021
Complete List of Authors:	Cheon, Seong Ik; Penn State University Park Batista Capaverde Silva, Leonardo; Penn State University Park Khair, Aditya; Carnegie Mellon, Chemical Engineering Zarzar, Lauren; Penn State

SCHOLARONE™
Manuscripts

1   **Interfacially-adsorbed particles enhance the self-propulsion of oil droplets in aqueous**
2   **surfactant**
3
4   Seong Ik Cheon[1], Leonardo Batista Capaverde Silva[2], Aditya S. Khair[3], Lauren D. Zarzar*[1,2,4]
5   1. Department of Chemistry, The Pennsylvania State University, University Park, PA 16802
6   2. Department of Materials Science and Engineering, The Pennsylvania State University,
7   University Park, PA 16802
8   3. Department of Chemical Engineering, Carnegie Mellon University, Pittsburgh, PA 15213
9   4. Materials Research Institute, The Pennsylvania State University, University Park, PA,
10   16802
11
12 *Correspondence to ldz4@psu.edu
13
14 **TOC**: The adsorption of solid particles on the surface of solubilizing oil droplets can significantly
15 enhance the droplets' self-propulsion speeds.
16
17 **Abstract**
18   Understanding the chemo-mechanical mechanisms that direct the motion of self-propulsive
19 colloids is important for the development of active materials and exploration of dynamic,
20 collective phenomena. Here, we demonstrate that the adsorption of solid particles on the surface
21 of solubilizing oil droplets can significantly enhance the droplets' self-propulsion speeds. We
22 investigate the relationship between the self-propulsion of bromodecane oil droplets containing
23 silica particles of varying concentration in Triton X-100 surfactant, noting up to order of magnitude
24 increases in propulsion speeds. Using fluorescently labeled silica, we observe packing of the
25 particles at the oil-water interfaces of the rear pole of the moving droplets. For bromodecane oil
26 droplets in Triton X-100, the highest droplet speeds were achieved at approximately 40% particle
27 surface coverage of the droplet interface. We find particle-assisted propulsion enhancement in
28 ionic surfactants and different oil droplet compositions as well, demonstrating the breadth of this
29 effect. While a precise mechanism for the propulsion enhancement remains unclear, the simple
30 addition of silica particles to droplet oil-water interfaces provides a straightforward route to tune
31 active droplet dynamics.
32
33 **Introduction**
34   Understanding and developing chemo-mechanical mechanisms to direct the motion of
35 colloids is a growing interest area in the field of active matter(1,2). An important consideration
36 when designing chemotactic active colloids is the mechanism by which asymmetric forces will be
37 generated and applied to direct the particle motion. Perhaps the most common approach is to create
38 Janus particles wherein the asymmetry is permanently built into the particle, such as having sides
39 of differing surface chemistry or anisotropic shape(3). However, isotropic colloids, such as
40 spherical liquid droplets, can also propel when exposed to chemical gradients in the
41 surroundings(4). In the case of active droplets, motion is typically driven by interfacial tension
42 gradients and Marangoni flows induced by interfacial reactions(5,6) or by micelle-mediated
43 solubilization, a process wherein the droplet contents are transferred into the continuous micellar
44 phase(7). It has been proposed that the solubilizate-surfactant interactions and the "filling" of the
45 surfactant micelles correspond to increased interfacial tensions at the droplet surface, and thus
46 droplets propel towards regions of "empty" micelles(2,8,9). For an isotropic droplet to move via

47 chemotaxis, asymmetry in the chemical gradient across the droplet surface must be maintained,
48 such as by feedback processes involving advective transport dominating over diffusion (e.g. high
49 Péclet number)(10), an externally applied chemical gradient(9,11) or the presence of another
50 nearby droplet that modifies the chemical gradient symmetry(8,12). Exploring mechanisms by
51 which to impose asymmetry into active colloids is an important step towards controlling properties
52 such as propulsion speed, sensitivity, directionality, and energy efficiency.
53 In this work, we explore the effect of particles adsorbed at droplet oil-water interfaces on
54 the self-propulsive behaviors of solubilizing oil droplets in nonionic and ionic surfactant solutions.
55 It is well known that particles can adsorb to liquid-liquid interfaces, such as in Pickering
56 emulsions(13,14). We demonstrate that interfacial adsorption of particles can lead to significant
57 increases in droplet speed, often by over an order magnitude, compared to self-propulsion of
58 solubilizing droplets without particles. We visualized fluorescently-labeled silica particles during
59 the droplet propulsion and determined that the particles pack together to create a cap on the rear
60 pole of the droplet. The degree of surface coverage by this particle cap influenced the droplet speed
61 in a non-monotonic fashion. Bromodecane droplets in Triton X-100 surfactant exhibited the
62 highest speed enhancement when silica particles covered roughly 40% of the droplet surface.
63 Droplets which solubilize but do not self-propel, such as bromooctane in 0.5 wt% Triton X-100,
64 can also be induced to rapidly swim via the addition of surface-active particles. The simple addition
65 of particles to droplet surfaces thus expands our ability to not only tune droplet propulsion speeds,
66 but also broadens the chemical compositions which can be used to create active droplets. These
67 advances may inspire new design approaches for active colloidal swimmers.
68
69 **Experimental**
70 **Materials**: Fumed silica particles were generously provided by Wacker Chemie (products
71 HDK S13, HDK H13L, HDK H20RH). The S13 silica had no surface modification, H13L had
72 50% surface coverage of dimethylsiloxy groups, and H20RH silica had 75% surface coverage of
73 long (~16 carbons on average) saturated hydrocarbon chains. These fumed silica particles are
74 amorphous aggregates with sizes ranging from $100 - 500$ nm with primary particles of 5-50 nm as
75 reported by the supplier. Other chemicals used include aminopropyl triethoxysilane (APTES)
76 (TCI, 96%), 1-ethyl-3-(3-dimethylaminopropyl) carbodiimide (EDC) (Chem Impex Int'l, 99.8%),
77 2-morpholinoethanesulfonic acid (MES) (Chem Impex Int'l, 99.8%), *N*-hydroxysuccinimide
78 (NHS) (Chem Impex Int'l, 99.5%), Fluorescein sodium salt (Fluka), bromooctane (Alfa Aesar,
79 98%), bromodecane (Frontier Scientific, 98%), bromododecane (Alfa Aesar, 98%),
80 bromohexadecane (TCI, 96%), brominated vegetable oil (Spectrum), Triton X-100 (TX) (Alfa
81 Aesar), sodium dodecyl sulfate (SDS) (Sigma Aldrich, 99%), cetyltrimethylammonium bromide
82 (CTAB) (Sigma Aldrich). All chemicals were used as received without further purification.
83 **Preparation of oil-in-water emulsions.** Silica particles were first dispersed in oil using a
84 probe sonicator (QSonica Q700). These dispersions were immediately used to fabricate droplets.
85 Unless specified otherwise, droplets were made with a volume ratio of 1:10 oil to surfactant
86 solution and were emulsified using a Vortex Genie 2 at its maximum setting (3200 RPM) for 3-5
87 seconds in 1-dram glass vials. Given that bulk emulsification was used, the droplets had a resultant
88 dispersity in size as well as particle concentration in each droplet.
89 **Brightfield and fluorescence microscopy.** To visualize the droplets, 0.5 µL of droplets
90 were pipetted into a glass-bottom dish containing surfactant solution. Droplets were gently agitated
91 to disperse them randomly within the dish. Videos of the droplet motion were taken using a Nikon
92 Ti-U inverted microscope and an Andor Zyla 4.2P camera. Typically, several videos for each set

93   of sample conditions were taken and analyzed to provide sufficient statistical data on droplet
94   speeds and particle surface coverages. Fluorescence images were collected with excitation
95   (AT480/30x) and emission (AT535/40m) filters.
96   **Analysis of droplet speed:** The videos for speed analysis were taken with a 6x
97   magnification, 1024 x 1024 resolution, and 30 fps using an Andor Zyla 4.2P camera. Instantaneous
98   droplet speed was analyzed with a MATLAB program as reported previously(8,15). An average
99   speed was assigned to a sample by averaging the maximum speeds of all the droplets captured
100 within a video. We report the average of the maximum speed and the standard deviation of the
101 maximum speed as seen in **Figure 1** and **Figure 5**. For the data presented in **Figure 3**, each data
102 point represents the maximum speed attained for a single droplet while it was imaged such that we
103 could correlate that speed directly with a particle surface coverage value. Please note that we did
104 not attempt to account for drift velocity due to convection in any of our reported speed
105 measurements. In our experience, drift velocity is less than 10 µm/s which is much slower than the
106 self-propelled droplets that can move upwards of 200 µm/s.
107   **Particle surface functionalization with fluorescein to create fluorescently labeled**
108 **particles.** *Functionalization of S13 with APTES.* In a 25 mL round bottom flask, 250 mg of dry
109 S13 particles were dispersed in 10 mL of acetone. 100 µL of 30 wt% ammonium hydroxide in
110 water was then added, followed by 300 µL of APTES. The flask was then sealed with a septum
111 and sonicated in a bath sonicator (Branson 1510) for 1 hour. The solution was then diluted with
112 acetone to a volume of 30 mL and centrifuged at 7,100 RCF for 10 minutes. The supernatant was
113 decanted and the particles were re-dispersed in acetone through sonication and centrifuged again
114 at 7,100 RCF for 10 minutes to pellet the particles. The supernatant was discarded, and the
115 nanoparticle pellet was collected and dried overnight. The particles were redispersed in 25 mL of
116 MES buffer (0.5 M, pH 5) for use in the following step. *Carbodiimide coupling of fluorescein and*
117 *amine terminated S13*. 125 mL of MES buffer (0.5 M, pH 5) was added to a 250 mL flask, followed
118 by 342.1 mg of fluorescein sodium salt, 165.9 mg of EDC, and 246 mg of NHS. The solution was
119 stirred at room temperature for 30 minutes, and then the 25 mL MES solution of amine-
120 functionalized S13 particles was added. The flask was sealed using a septum, covered in foil, and
121 left to react at room temperature for 24 hours while stirring. The solution was then diluted with
122 acetone and excess reagents were removed similarly to the previous step by using centrifugation,
123 washing, and drying. The particles were dispersed in 10 mL of hexane for use in the following
124 step. *Making florescent particles hydrophobic*. The 10 mL of fluorescein-functionalized particles
125 were added to a 25 mL round bottom flask followed by 200 µL of diethylamine and 1.5 mL of
126 hexadecyltriethoxysilane. The flask was sealed with a septum and left to react for 24 hours while
127 stirring and covered with foil. The solution was then diluted with acetone and excess reagents were
128 removed similarly to the previous steps by using centrifugation, washing, and drying, ultimately
129 producing hydrophobic, fluorescent fumed silica.
130   **Thermogravimetric analysis (TGA) of dry, functionalized silica particles.** The weight loss
131 of functionalized silica particles was monitored by TGA (Discovery Series TGA Q5500)(16,17).
132 TGA traces taken for particles produced after each functionalization step are shown in **Figure S1.**
133 The silica particles were heated in air from 25 °C to 120 °C at 10 °C/min and held in isotherm for
134 10 minutes to remove residual solvent. Particles are then heated to 800 °C at 20 °C/min. The
135 normalized weight loss was then calculated from mass change between 120 °C and 800 °C.
136   **Analysis of particle surface coverage on droplets:** Surface coverage of droplets coated with
137 fluorescent silica nanoparticles were determined from fluorescence images of the droplets. We
138 approximated the particle coverage as a symmetric, spherical cap of particles. From the images,

139   droplet radius and cap radius are measured to calculate the approximate surface coverage of
140   droplets, as shown in **Figure 2**. There is notable error inherent within this approximation, given
141   that the particles are not distributed evenly throughout the cap or cap edges, the surface aggregates
142   can become rough or non-spherical due to particle packing, and some distortion in the images is
143   created due to droplet motion during the image exposure, which was necessarily long $(30 - 60$ ms$)$
144   to capture sufficient fluorescence intensity.

145

146   **Results and Discussion**
147   To test whether particles at droplet interfaces might influence self-propulsion of
148   solubilizing oil droplets, we began by examining the effect of partially hydrophobic silica particles
149   on the swimming speeds of 1-bromodecane droplets in aqueous Triton X-100 (hereafter, TX). TX
150   is a nonionic surfactant which has previously been shown to generate active oil droplets via
151   micelle-mediated solubilization(8). Bromodecane was chosen because it is an oil with low water
152   solubility, such that solubilization is expected to be micelle-mediated(8), and it is denser than water
153   such that the droplets sink to the bottom substrate, lending to ease of experimentation. We chose
154   partially hydrophobized fumed silica particles (H13L produced by Wacker Chemie, 150-500 nm,
155   50% coverage with dimethylsiloxy groups and 50% residual surface silanols) to favor particle
156   wetting by both oil and water and enhance interfacial activity; these particles are, however, still
157   preferentially dispersible in the oil phase. We prepared polydisperse bromodecane droplets with
158   and without 0.5 wt% H13L particles in 0.1 wt% TX by vortex mixing and examined the droplet
159   dynamics using optical microscopy and droplet tracking analysis (refer to Methods Section for
160   details). Droplets were polydisperse but typical diameters of droplets that were analyzed fell in the
161   range of $20 - 100$ µm. The bromodecane droplets without particles moved slowly, no more than 3
162   µm/s (**Figure 1a, left**). However, droplets with the silica particles were self-propelled and moved
163   significantly faster, on the order of 50 µm/s, rapidly careening through the imaging chamber
164   (**Figure 1b, Video S1**). Qualitatively, it was evident from these initial experiments that the
165   particles had a notable effect on the droplet dynamics.
166   In order to quantify the relationship between particle concentration, surfactant
167   concentration, and droplet speed, we conducted a series of experiments with aqueous TX surfactant
168   concentrations between 0.1 wt% and 1 wt% and H13L particle concentrations in bromodecane
169   between 0 wt% and 2 wt%. For each sample, we used a standardized procedure in which a small
170   number of droplets (typically less than 20 droplets in 0.5 µL of solution) were extracted from the
171   emulsion sample vial and added to a glass-bottom dish containing 1 mL the same surfactant
172   concentration in which the droplets were prepared. The solution was gently agitated to randomly
173   disperse the droplets, and videos of the droplets were collected over 60 seconds. Droplet
174   trajectories and instantaneous speeds were analyzed using Matlab image analysis(8,15). Given that
175   the droplets often swam in curved trajectories and exhibited variation in instantaneous speed that
176   was dependent on the path, we used the maximum speed each droplet reached during the video as
177   the basis for comparison. Averages and standard deviations for the resultant maximum speeds for
178   each set of experimental conditions are given in **Figure 1b** and **Table S1**. Droplets exhibited faster
179   speeds in higher surfactant concentrations for a given particle concentration. These trends with
180   surfactant concentration are consistent with a solubilization-driven, micelle-mediated propulsion
181   mechanism(2). Higher particle concentration, however, did not always correlate to faster speeds,
182   and instead there was a maximum in droplet speed at intermediate particle concentrations (**Figure
183   1b**). The particle concentration yielding the fastest speeds varied slightly as a function of TX
184   concentration with the droplet speed peaking at around 0.2 wt% to 0.5 wt% H13L particles. At

185 lower particle concentrations, we could not see the particles clearly within the droplets, but at
186 higher particle concentrations, we observed large irregular particle aggregates on the droplets'
187 surfaces (**Figure 1b inset**). We suspected that the particle concentration in the droplet was
188 correlated with the number of particles at the droplet interface and the total displaced oil-water
189 interfacial area, which was, in turn, affecting the droplet speeds.
190   To directly correlate the particle concentrations to droplet interfacial coverage and speeds,
191 we needed to be able to directly visualize the particles at the droplet surface, such as with
192 fluorescence. We aimed to modify the fumed silica particles with a fluorescent dye, fluorescein,
193 while still retaining a particle surface activity similar to that of the H13L (**Figure 2a**). Starting
194 from pristine hydrophilic fumed silica, we functionalized the silanol surface with aminopropyl
195 triethoxysilane (APTES) and then coupled the surface amine with the carboxylic acid of
196 fluorescein sodium salt via carbodiimide coupling chemistry using 1-ethyl-3-(3-
197 dimethylaminopropyl) carbodiimide (EDC) and *N*-hydroxysuccinimide (NHS). At this stage, the
198 particles were still hydrophilic and dispersed easily in water, so we further functionalized
199 remaining surface silanol groups with hexadecyltrimethoxysilane to render the particles more
200 hydrophobic. After functionalization, the particles were fluorescent and dispersible in the
201 bromodecane. Please refer to the Methods section for specific reaction details and particle surface
202 analysis.
203   To test if the hydrophobized fluorescent silica could be used for particle visualization, the
204 particles were dispersed into bromodecane at 2 wt% and emulsions were prepared by vortex
205 mixing the bromodecane/particle mixture in 0.5 wt% TX. Immediately upon placing the droplets
206 into fresh surfactant solution for imaging, the droplets were non-mobile and most of the fluorescent
207 particles were dispersed inside the droplets. Over a short time, particles that were circulating inside
208 the droplets began to accumulate at the droplet surface and aggregate, eventually being pushed
209 towards the rear pole of the droplet as the droplet started to propel quickly forward (**Figure 2b**,
210 **Video S2**). Using the fluorescent particles, we could visualize the degree of droplet interfacial
211 coverage once the droplets reached a steady-state speed, which we approximated from the
212 micrographs as the surface area of a spherical cap (**Figure 2b**). This is a rough estimate, as the
213 particles were not perfectly packed at the interface, the edges of the particle cap were not straight,
214 and we could not visualize the 3D surface coverage around all sides of the droplet simultaneously.
215 There was also some image blur in the fluorescence micrographs because the droplets were moving
216 during the camera exposure time, which was necessarily long (30 – 60 ms) in order to capture
217 sufficient light intensity to visualize the fluorescent particles.
218   Despite the approximations necessary to quantify surface coverage, we could still visualize
219 the particles sufficiently to correlate the particle coverage with droplet behavior. Bromodecane
220 droplets with fluorescent particle concentrations in the range of $0.2 - 2$ wt% were prepared in 0.5
221 wt% TX and videos of the droplets under both brightfield and fluorescence were collected (see
222 **Video S3** as an example of a fluorescence video). From these videos, both speed and surface
223 coverage were measured for individual droplets; surface coverages were converted to cap coverage
224 angle, θ_c, where θ_c=0° is an uncovered droplet and θ_c=180° is a fully covered droplet. The speed
225 of the droplets as a function of the coverage angle and particle concentration is shown in **Figure
226 3a**. Droplet speed showed a non-monotonic dependence on particle coverage with the propulsion
227 speed lowest at small ($\theta_c \approx 0°$) and large ($\theta_c \approx 180°$) surface coverages. The maximum speed
228 attained was in the range of about 300 μm/s at approximately 40% surface coverage, with θ_c just
229 below 90°. Particle concentrations correlated roughly with surface coverage, as expected based on
230 the data in **Figure 1b**, although there was still notable variation likely due to dispersity in the

231   numbers of particles within each droplet resultant from the preparation method. The fact that there
232   exists significant variation in surface coverage as a function of initial particle concentration in the
233   bromodecane also explains the relatively large error bars of **Figure 1b**.
234   The evolution of droplet speed as a single droplet solubilizes over time in 0.5 wt% TX is
235   shown in **Figure 3b**. With moderate starting surface coverage ($\theta_c \approx 50°$), the droplet initially
236   propelled at ~250 μm/s and maintained a similar speed for about 30 minutes, at which point the
237   speed began to decrease until eventually the droplet was nonactive and completely coated with
238   particles. The surface area of the initial particle patch was estimated to be approximately 11,600 μ
239   m^2 and the surface area of the final, fully-covered droplet was estimated to be approximately
240   10,200 μm^2; this indicates that the vast majority of particles are irreversibly adsorbed such that as
241   the droplet volume shrinks, the total surface coverage by particles stays constant and the percent
242   surface coverage increases. A small decrease in particle-covered surface area might be attributed
243   to adsorbed particles jamming more tightly. Using the trajectory from **Figure 3b**, we estimate that
244   this droplet had a cruising range of about 0.8 meter over its lifetime of an hour. Droplets with
245   different starting surface coverages or droplet volumes would have different cruising ranges.
246   We consider the following framework to conceptually rationalize the trends observed in
247   the data of **Figure 3**. The measured propulsion speed is around 300 $\mu m/s$ for a half-coated droplet,
248   which, upon using a droplet radius $a_{drop} = 50\ \mu m$ and kinematic viscosity of $1\frac{\mu m^2}{s}$, gives a
249   Reynolds number $Re = 1.5 \times 10^{-2}$. Thus, the droplet motion is in the creeping flow, or low
250   Reynolds number, regime. The oil undergoes solubilization into the aqueous solution, through the
251   formation of oil-filled micelles that are stabilized via uptake of surfactant monomer adsorbed at
252   the oil-water interface. We assume that the flux j_m of oil filled micelles into the aqueous solution
253   is constant. A mass balance on the oil in the drop shows that $j_m = -\left(\frac{1}{V_m}\right)\frac{da_{drop}}{dt}$, where a_{drop} is the
254   radius of the oil drop, V_m is the volume of an oil filled micelle, and t is time. The rate of change
255   of the drop radius is small, $O(0.01\ \mu m/s)$, compared to the propulsion velocity observed in
256   experiments, $O(100\ \mu m/s))$; hence, the drop radius is assumed to be essentially constant during
257   propulsion. The solubilization consumes adsorbed surfactant at a rate dj_m, where d is the number
258   of surfactant monomers per oil filled micelle, or aggregation number. Replenishment of surfactant
259   at the oil-water interface occurs via adsorption of monomers from the bulk solution. The bulk
260   concentration of surfactant monomer is expected to remain uniform and equal to the critical micelle
261   concentration (C_{CMC}) during the solubilization process, as a result of an abundance of empty
262   micelles that, via rapid dissociation, rectify the deficit in bulk surfactant concentration due to
263   adsorption(18).
264   The concentration of adsorbed surfactant may vary along the droplet surface via surface
265   diffusion and advection with the local interfacial fluid flow. Such variation will lead to gradients
266   in surface tension along the oil-water interface that, in turn, drive Marangoni stresses, potentially
267   causing droplet propulsion. The droplets propel with the particle-uncoated portion of their surface
268   facing forward (**Figure 2b, Figure 3**). We therefore expect that there is a gradient of adsorbed
269   surfactant along the droplet interface, where the adsorbed surfactant concentration is highest at the
270   front of the drop and lowest towards the rear. The surface tension therefore follows the opposite
271   trend: highest at the back and lowest at the front. Thus, Marangoni stresses drive an interfacial
272   flow toward the back of the droplet (i.e., the interface is "pulled" backward by the higher interfacial
273   tension at the rear of the drop).

274   The relative importance of surface diffusion to advection is characterized by a Péclet
275   number $Pe = Ua/D_s$, where U is the propulsion speed of the drop, and D_s is the surface diffusion
276   coefficient. Using a typical speed $U = 100\ \mu m/s$, drop size $a_{drop} = 50\ \mu m$, and $D_s = 150\ \mu m^2/s$
277   yields $Pe = 33$. (We have assumed, in the absence of better information, that the surface diffusion
278   coefficient of surfactant monomer is equal to the bulk diffusion coefficient(19).) Hence, advection
279   dominates diffusion. In this regime, it has recently been predicted that droplets in a micellar
280   solution (with bulk surfactant concentration above the C_{CMC}) can spontaneously self-propel due to
281   a Marangoni instability(18), resulting from the nonlinear dependence of the advective interfacial
282   flux of surfactant on the interfacial velocity and surfactant concentration. A similar self-propulsion
283   mechanism for a solid particle coated by enzymes that are mobilized by diffusiophoretic flows,
284   generated by a concentration gradient in the product species of the enzymatic reaction, has also
285   recently been proposed(20).
286   Indeed, the particle-free (0 wt%) bromodecane droplets in **Figure 1** do exhibit self-
287   propulsion at the higher surfactant concentrations, which we believe is due to a Marangoni
288   instability as reported by many researchers(7,21). However, it is important to note that even
289   stationary droplets, such as the particle-free bromodecane in 0.1 wt% TX, still generate fluid
290   pumping from top to bottom, as visualized using side-oriented transmission optical microscopy
291   (**Video S4**). Here, the asymmetry that induces the interfacial flows is imposed by the presence of
292   the substrate, where there is a sustained, higher concentration of oil and higher interfacial tension
293   at the droplet bottom (**Figure 4a**). The solubilized oil gradients are axially symmetric so there is
294   no net lateral Marangoni force and the droplet does not translate (i.e. is not self-propelled). The
295   vertical Marangoni force is counterbalanced by gravity. While these "top to bottom" flows do not
296   generate lateral force, they can lead to, and are necessary for, the initial packing of the silica
297   particles along the droplet surface which we believe is the first step in inducing particle-enhanced
298   propulsion.
299   We propose that the addition of particles leads to an enhancement in self-propulsion by
300   breaking the symmetry of the interfacial Marangoni flow that is otherwise axially symmetric about
301   the vector perpendicular to the substrate (**Figure 4b**). Interfacial flows, present even in stationary
302   solubilizing droplets, serve to advect interfacially-adsorbed particles and pack them to form a cap.
303   In this cap region, it is still unclear precisely how the particles are affecting the interfacial tension
304   gradients, but it appears that an inhomogeneous distribution of particles within the cap can lead to
305   spontaneous cap rotation; once the cap rotates, now the Marangoni force has a lateral component
306   that drives the droplet to propel sideways (**Video S5**). A droplet with a particle cap that is axially
307   symmetric about the vector perpendicular to the surface still pumps fluid from top to bottom at a
308   rate similar to the non-coated drop and remains stationary; the tilting of the particle cap relative to
309   the substrate appears key to lateral motion, as observed with side-view transmission optical
310   microscopy (**Video S6**). Future research will be necessary to fully understand the role of particles
311   in inducing the cap rotation and enhanced lateral propulsion.
312   To explore the generality of this particle-assisted propulsion, we examined the swimming
313   behaviors of bromodecane in several different surfactants and surfactant concentrations.
314   Bromodecane droplets containing 1 wt% fluorescent particles were emulsified in anionic sodium
315   dodecyl sulfate (SDS), cationic cetyl trimethyl ammonium bromide (CTAB), and nonionic TX of
316   varying concentration. Individual droplets within each sample were tracked and characterized to
317   determine their maximum speed and particle coverage. Only droplets that had between 30% and
318   50% surface coverage were included in the data shown in **Figure 5** and **Table S2-S3** to account
319   for possible differences in particle surface activity under the varying surfactant conditions(22).

320   Without particles, bromodecane droplets had slow swimming speeds in all concentrations of the
321   ionic surfactants, SDS and CTAB, (< 20 μm/s), although the bromodecane was solubilizing at a
322   noticeable rate (0.03 and 0.06 μm/min respectively, **Table S4**). Inclusion of particles increased the
323   droplet speed by over an order of magnitude for many conditions (**Video S7**), and the enhancement
324   increased at higher SDS and CTAB concentrations. Addition of 0.25 M NaCl to 1 wt% and 5 wt%
325   SDS or 1 wt% and 2.5 wt% CTAB marginally increased droplet speeds without particles and also
326   increased solubilization rates slightly, potentially due to screening of the electrostatic repulsion
327   between the charged micelles and interface (**Table S2, S4**). Addition of salt in the presence of
328   particles, however, led to significantly faster droplet speeds in 1 wt% SDS-particles-salt (345.9 ±
329   74.4 μm/s) and in 1 wt% CTAB-particles-salt (251.6 ± 42.9 μm/s). Adding salt did not
330   significantly influence the speed of droplets in nonionic surfactant TX-stabilized droplets with or
331   without particles. These results suggest that salt affects the propulsion via surfactant-salt
332   interactions or surfactant-particle-salt interactions, rather than just interactions between the salt
333   and particles alone. In the case of SDS and CTAB, addition of salt may also cause a change in the
334   CMC(23,24), and salt also may also allow the particles to pack together more tightly by screening
335   charge on the fumed silica resulting from ionic surfactant-particle association(25).
336   Given that the oil droplets are propelled by interfacial tension gradients resultant from oil-
337   surfactant interactions, we wondered to what extent oil droplets of varying chemistry and
338   solubilization rates would be influenced by particles. We measured the speeds of 1-bromooctane,
339   1-bromodecane, 1-bromododecane, 1-bromohexadecane, and brominated vegetable oil droplets
340   with and without 1 wt% fluorescent particles in 0.5 wt% TX (**Figure 5b**, **Table S3**). Again, we
341   only consider here droplets with particle surface coverage in the range of 30-50%. All oils except
342   the brominated vegetable oil exhibited enhanced propulsion speeds with particles present. Without
343   particles, the solubilization rates of these oils are 0.41, 0.24, 0.13, <0.01, and <0.01 μm/min,
344   respectively, where the bromohexadecane and brominated vegetable oil did not solubilize to a
345   measurable extent within one hour (**Table S4**). We do believe, however, that the bromohexadecane
346   still solubilizes, albeit at a slow rate, given previous reports of measurable solubilization of
347   hexadecane in TX(26). Brominated vegetable oil is quite viscous containing molecules of high
348   molecular weight and is thus expected to solubilize even more slowly than the bromohexadecane;
349   brominated vegetable oil droplets do not even form a particle cap. This observation is consistent
350   with the idea that solubilization and the generation of oil gradients is a requirement for sustaining
351   interfacial Marangoni flow that initially packs the particles at the droplet interface and leads to
352   propulsion; while particles can significantly enhance the speed of droplets that undergo some
353   degree of solubilization, particles alone cannot generate propulsion in the absence of
354   solubilization.

356   **Conclusion**
357   In summary, we have demonstrated that adsorption of silica nanoparticles at the interface
358   of a solubilizing oil droplet in surfactant solution can significantly accelerate the droplets' self-
359   propulsion speed. The polarization of the particles across the droplet surface arises spontaneously
360   to form a cap, and using fluorescent particle visualization, we correlated the degree of particle
361   surface coverage on bromodecane droplets to the droplet speed in TX surfactant. Slowest speeds
362   were found at the lowest and highest surface coverages and the fastest speeds were achieved at
363   intermediate surface coverages of about 40%. The particle-assisted propulsion acceleration was
364   further demonstrated in nonionic, anionic, and cationic surfactants and a range of oils with varying
365   solubilization rates. Future work will include development of fluid mechanical models to

understand the role of interfacially adsorbed particles on the droplet behaviors. Approaches by which to modulate the distribution of solubilization and interfacial flow across droplet interfaces, such as by addition of particles, may provide a facile route to tuning active colloid speeds and dynamics. Further exploration involving stimuli-responsive particles(27) or droplets containing multiple oils(28) with particles at droplet-internal oil-oil interfaces(29) may provide new opportunities for tuning the behaviors of swimming droplets.
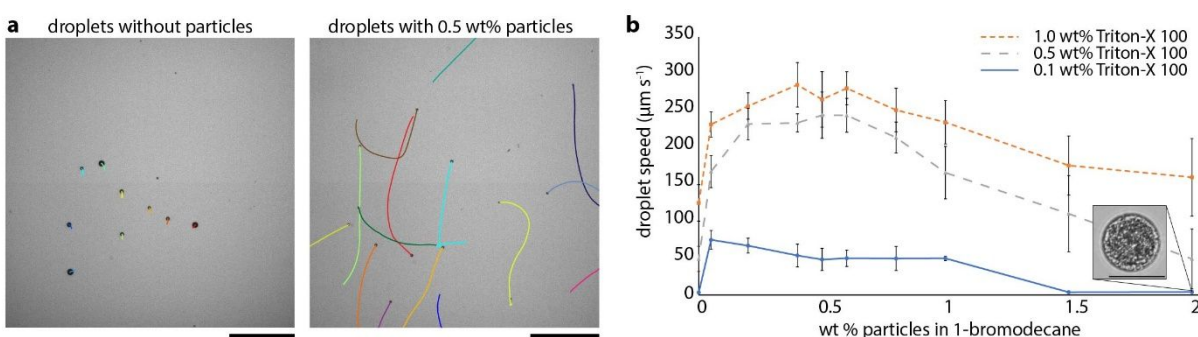
Figure 1. Silica particles affect the self-propulsion of oil droplets in surfactant solution. **a.** 1-Bromodecane oil droplets without particles and with 0.5 wt% H13L silica were dispersed in 0.1 wt% TX and the droplet trajectories were analyzed. Shown are the droplet trajectories over a 60 second period. Droplets without particles were not active, and droplets with particles swam much faster, reaching peak speeds of about 50 µm/s. Scale, 1 mm. **b.** The speed of bromodecane droplets was investigated for various aqueous TX concentrations and H13L particle concentrations. The speed of a droplet was defined as the maximum speed reached during the droplet's lifetime in the video frame. Data shown represent the average and standard deviation for a sample size of at least 10 droplets per experimental condition. The inset shows an optical micrograph of a droplet at 2 wt% particle concentration in 0.1 wt% TX where the packing of the nanoscale particles at the droplet surface become visible, showing high surface coverage. When higher concentrations of TX surfactant are used, we do not often see such fully packed surfaces and the droplets may experience significant motion even at 2 wt% particles. Scale, 50 µm.
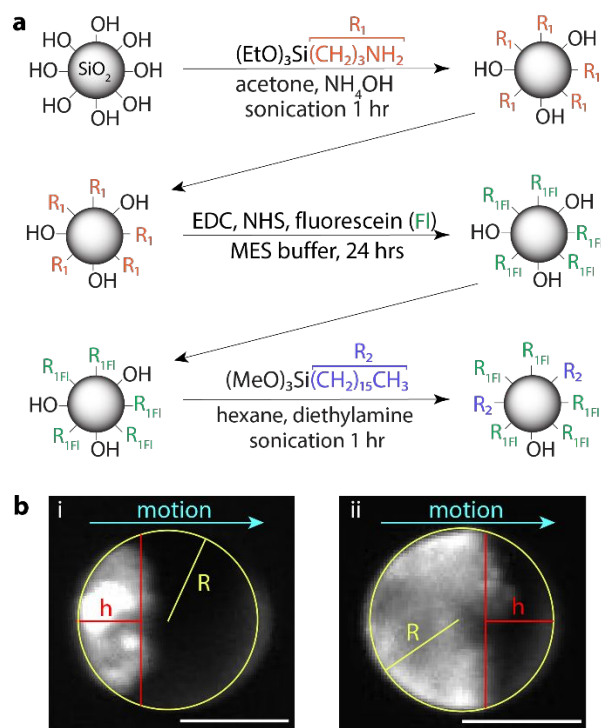
Figure 2. Fluorescence visualization of particles at droplet interfaces. a. Schematic describing the preparation of fluorescent, hydrophobic fumed silica. **b.** The particle surface coverage of a droplet was estimated using fluorescence micrographs. Fluorescence images of two different droplets, both prepared with 1 wt% fluorescent particles in bromodecane with 0.5 wt% TX, are shown as examples. Overlaid diagrams illustrate how particle surface coverage was estimated by assuming a spherical cap, where h is the height of the cap and R is the radius of the droplet (and cap). For (i), estimated fractional surface coverage $= h/2R = 32\%$, and for (ii) fractional surface coverage $= 1 - h/2R = 70\%$. Scale, 50 μm.
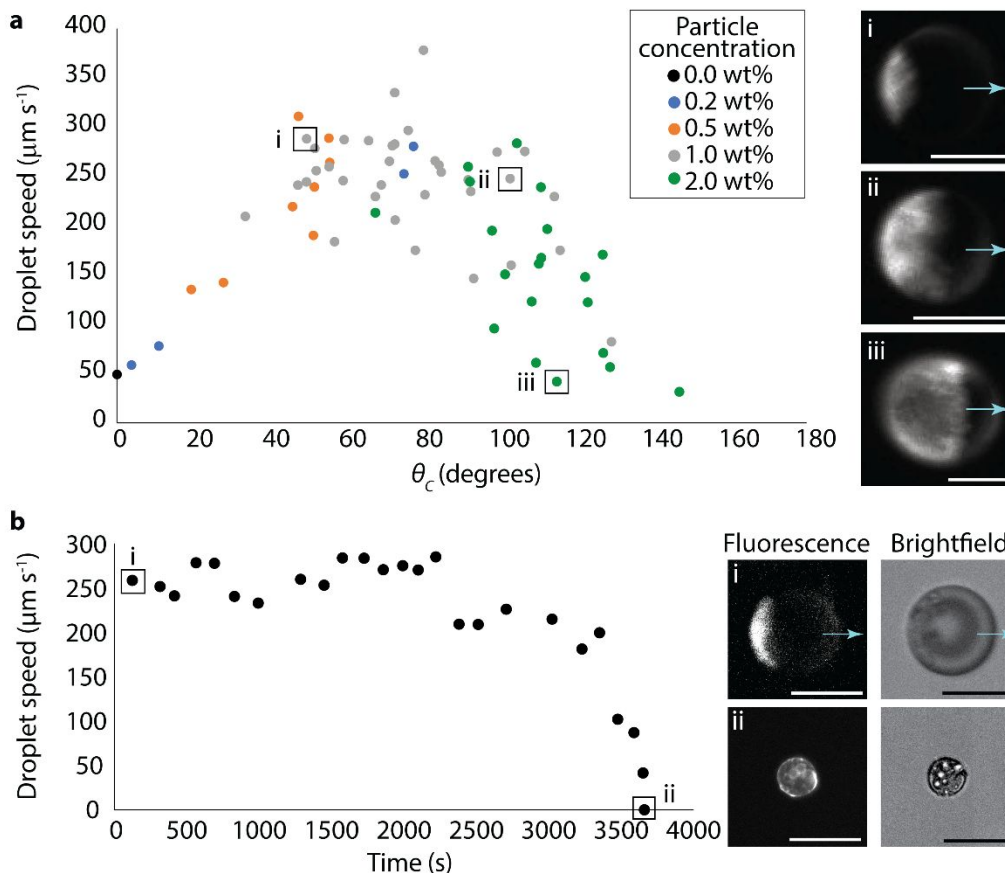
Figure 3. Degree of droplet surface covered by particles affects droplet speed. The scatterplot shows the relationship between bromodecane droplet speed and surface coverage with particles in 0.5 wt% TX. Surface coverage is plotted as coverage cap angle θ_c, where θ_c=0° corresponds to no particle coverage and θ_c=180° corresponds to complete coverage. Each datapoint represents a single droplet's surface coverage and highest speed reached during imaging. The color coding of the datapoints represents the initial concentration of particles used when preparing the droplet. Black = 0.0 wt%, blue = 0.2 wt%, orange = 0.5 wt%, grey = 1.0 wt%, and green = 2.0 wt% fluorescent particles in bromodecane. The initial particle concentration showed a general correlation with droplet surface coverage, where higher particle concentrations were more likely to produce droplets with higher surface coverages. Fluorescence micrographs of three exemplary droplets are shown and the arrows represent direction of droplet motion. Scale, 50 μm. **b.** The scatterplot shows the evolution of a single bromodecane droplet's speed over its lifetime of about an hour in 0.5 wt% TX. The droplet started with fast speeds and moderate particle coverage ($\theta_c \approx$ 50°). Over time, the particle coverage increased while the droplet volume decreased due to solubilization, until eventually the droplet motion ceased with $\theta_c \approx 180°$. Fluorescence and brightfield micrographs are given at right. The arrows represent the direction of droplet motion. Scale, 100 μm.
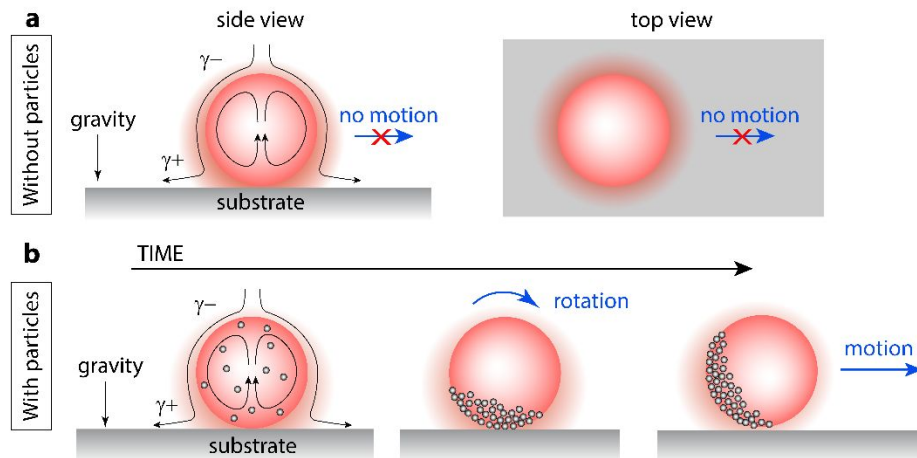
424
425 **Figure 4. Spontaneous polarization of particles on solubilizing oil droplet interfaces leads to**
426 **enhanced self-propulsion. a.** An oil droplet that solubilizes but does not self-propel can still
427 experience an interfacial tension gradient from top to bottom where the asymmetry is imposed by
428 the substrate. Solubilized oil builds up near the solid surface, generating Marangoni flows that
429 advect oil-free surfactant from above (side view). The droplet does not move laterally because the
430 oil solubilization is axially symmetric about the vector perpendicular to the surface (top view). $\gamma+$
431 indicates an elevated interfacial tension and $\gamma-$ indicates a lowered interfacial tension. See **Video**
432 **S4**. **b**. When particles are introduced, advection of the interfacially-adsorbed particles creates a
433 cap. Once the cap rotates, droplets move laterally; droplets move most quickly when the particle
434 cap is oriented perpendicular to the substrate. See **Videos S5-S6**.
435
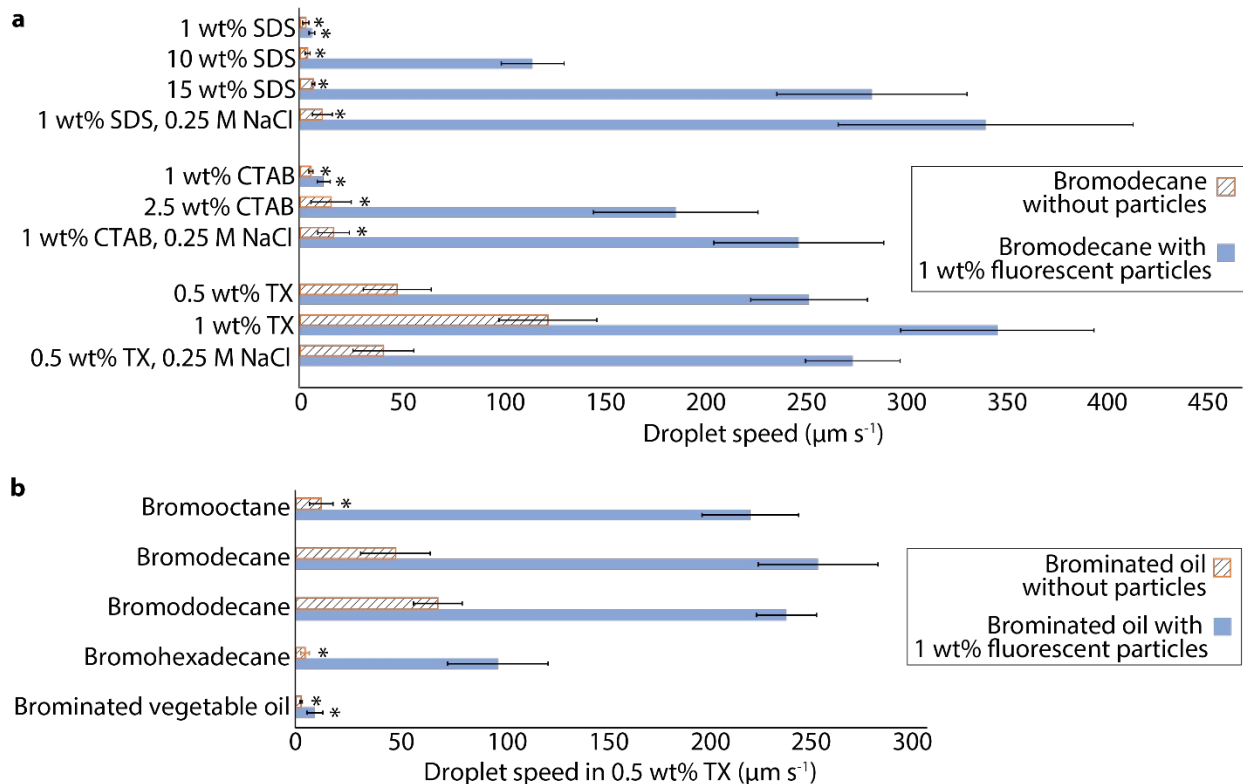
Figure 5. Enhanced self-propulsion of oil droplets of varying oil and surfactant chemistry. a. Speeds of bromodecane droplets with and without 1 wt% fluorescent silica particles were measured in different concentrations of SDS, CTAB, and TX surfactant, with and without NaCl. The asterisk (*) indicates that the droplets were noticeably drifting rather than self-propelling, as distinguished by the droplets all moving in the same direction. The speeds of droplets prepared with ionic surfactants, SDS and CTAB, were sensitive to the addition of 0.25 M NaCl, whereas droplets in nonionic TX were not. **b.** Speeds of various brominated oils with and without 1 wt% fluorescent silica particles were measured in 0.5 wt% TX. See **Table S4** for solubilization rates. All oils, except for brominated vegetable oil which had indetectable solubilization, showed significant enhancement in self-propulsion speed due to the surface adsorption of silica particles. Each bar shows the average and standard deviation of a minimum of 5 droplet measurements. The data plotted in (**a, b**) is tabulated in **Table S2, S3**. Only droplets with 30-50% surface coverage of particles were included in this data to account for possible differences in particle surface adsorption with variation in oil or surfactant.

References

1.   Dey KK, Sen A. Chemically Propelled Molecules and Machines. J Am Chem Soc. 2017;139(23):7666–76.

2.   Maass CC, Krüger C, Herminghaus S, Bahr C. Swimming Droplets. Annu Rev Condens Matter Phys. 2016;7(1):171–93.

3.   Pourrahimi AM, Pumera M. Multifunctional and Self-propelled Spherical Janus nano/micromotors: Recent Advances. Nanoscale. 2018;10(35):16398–415.

4.   Lach S, Yoon SM, Grzybowski BA. Tactic, Reactive, and Functional Droplets Outside of Equilibrium. Chem Soc Rev. 2016;45(17):4766–96.

462   5.   Toyota T, Maru N, Hanczyc MM, Ikegami T, Sugawara T. Self-propelled Oil Droplets
463   Consuming "Fuel" Surfactant. J Am Chem Soc. 2009;131(14):5012–3.
464   6.   Hanczyc MM, Toyota T, Ikegami T, Packard N, Sugawara T. Fatty Acid Chemistry At
465   The Oil-water Interface: Self-propelled Oil Droplets. J Am Chem Soc.
466   2007;129(30):9386–91.
467   7.   Izri Z, Van Der Linden MN, Michelin S, Dauchot O. Self-propulsion Of Pure water
468   droplets By Spontaneous Marangoni-stress-Driven Motion. Phys Rev Lett.
469   2014;113(24):1–5.
470   8.   Meredith CH, Moerman PG, Groenewold J, Chiu YJ, Kegel WK, van Blaaderen A, et al.
471   Predator–prey Interactions Between Droplets Driven By Non-reciprocal Oil Exchange.
472   Nat Chem [Internet]. 2020;12(12):1136–42. Available from:
473   http://dx.doi.org/10.1038/s41557-020-00575-0
474   9.   Jin C, Kru-ger C, Maass CC. Chemotaxis And Autochemotaxis Of Self-propelling Droplet
475   Swimmers. Proc Natl Acad Sci U S A. 2017;114(20):5089–94.
476   10.   Michelin S, Lauga E, Bartolo D. Spontaneous Autophoretic Motion Of Isotropic Particles.
477   Phys Fluids. 2013;25(6).
478   11.   Lagzi I, Soh S, Wesson PJ, Browne KP, Grzybowski BA. Maze Solving By Chemotactic
479   Droplets. J Am Chem Soc. 2010;132(4):1198–9.
480   12.   Moerman PG, Moyses HW, Wee EB Van Der, Grier DG, Blaaderen A Van, Kegel WK, et
481   al. Solute-mediated Interactions Between Active Droplets. Phys Rev E. 2017;96:032607.
482   13.   Binks BP, Horozov TS. Colloidal Particles At Liquid Interfaces. Cambridge University
483   Press. 2006.
484   14.   Binks BP. Colloidal Particles At A Range Of Fluid-Fluid Interfaces. Langmuir.
485   2017;33(28):6947–63.
486   15.   Crocker JC, Grier DG. Methods Of Digital Video Microscopy For Colloidal Studies. J
487   Colloid Interface Sci. 1996;179(1):298–310.
488   16.   Wisser FM, Abele M, Gasthauer M, Müller K, Moszner N, Kickelbick G. Detection Of
489   Surface Silanol Groups On Pristine And Functionalized Silica Mixed Oxides And
490   Zirconia. J Colloid Interface Sci [Internet]. 2012;374(1):77–82. Available from:
491   http://dx.doi.org/10.1016/j.jcis.2012.01.015
492   17.   Mueller R, Kammler HK, Wegner K, Pratsinis SE. OH Surface Density Of SiO2 And
493   TiO2 By Thermogravimetric Analysis. Langmuir. 2003;19(1):160–5.
494   18.   Morozov M. Adsorption Inhibition By Swollen Micelles May Cause Multistability In
495   Active Droplets. Soft Matter. 2020;16(24):5624–32.
496   19.   Fang XW, Zhao S, Mao SZ, Yu JY, Du YR. Mixed micelles of cationic-nonionic
497   surfactants: NMR self-diffusion studies of Triton X-100 and cetyltrimethylammonium
498   bromide in aqueous solution. Colloid Polym Sci. 2003;281(5):455–60.
499   20.   De Corato M, Pagonabarraga I, Abdelmohsen LKEA, Sánchez S, Arroyo M. Spontaneous
500   polarization and locomotion of an active particle with surface-mobile enzymes. Phys Rev
501   Fluids. 2020;5(12):1–11.
502   21.   Hokmabad BV, Dey R, Jalaal M, Mohanty D, Almukambetova M, Baldwin KA, et al.
503   Emergence of Bimodal Motility in Active Droplets. Phys Rev X [Internet].
504   2021;11(1):11043. Available from: https://doi.org/10.1103/PhysRevX.11.011043
505   22.   Katepalli H, Bose A. Response of Surfactant Stabilized Oil-in-Water Emulsions to the
506   Addition of Particles in an Aqueous Suspension. Langmuir. 2014;30:12736–42.
507   23.   Gurkov TD, Dimitrova DT, Marinova KG, Bilke-Crause C, Gerber C, Ivanov IB. Ionic

508 Surfactants On Fluid Interfaces: Determination Of The Adsorption; Role Of The Salt And
509 The Type Of The Hydrophobic Phase. Colloids Surfaces A Physicochem Eng Asp.
510 2005;261(1–3):29–38.
511 24. Mahbub S, Molla MR, Saha M, Shahriar I, Hoque MA, Halim MA, et al. Conductometric
512 And Molecular Dynamics Studies Of The Aggregation Behavior Of Sodium Dodecyl
513 Sulfate (SDS) And Cetyltrimethylammonium Bromide (CTAB) In Aqueous And
514 Electrolytes Solution. J Mol Liq [Internet]. 2019;283:263–75. Available from:
515 https://doi.org/10.1016/j.molliq.2019.03.045
516 25. Wang H, Singh V, Behrens SH. Image Charge Effects On The Formation Of Pickering
517 Emulsions. J Phys Chem Lett. 2012;3(20):2986–90.
518 26. Zhong H, Yang L, Zeng G, Brusseau ML, Wang Y, Li Y, et al. Aggregate-based sub-
519 CMC solubilization of hexadecane by surfactants. RSC Adv. 2015;5(95):78142–9.
520 27. Tang J, Quinlan PJ, Tam KC. Stimuli-responsive Pickering Emulsions: Recent Advances
521 And Potential Applications. Soft Matter [Internet]. 2015;11(18):3512–29. Available from:
522 http://xlink.rsc.org/?DOI=C5SM00247H
523 28. Balaj R V., Zarzar LD. Reconfigurable Complex Emulsions: Design, Properties, And
524 Applications. Chem Phys Rev. 2020;1(1):011301.
525 29. Cheon SI, Batista Capaverde Silva L, Ditzler R, Zarzar LD. Particle Stabilization of Oil–
526 Fluorocarbon Interfaces and Effects on Multiphase Oil-in-Water Complex Emulsion
527 Morphology and Reconfigurability. Langmuir. 2020;36:7083–90.
528